Theoretical derivation and a single abrasive particle on material removed of slicing ceramic

Yao-Yang Tsai[1], Ming-Chang Wu[2], Yunn-Shiuan Liao[1], Chung-Chen Tsao[2,*], Chun-Yao Hsu[2,*]
[1]Department of Mechanical Engineering, National Taiwan University, Taipei 10617, Taiwan
[2]Department of Mechanical Engineering, Lunghwa University of Science and Technology, Taoyuan 33306, Taiwan

Abstract

Multi-wire saw machining (MWSM) used for slicing hard-brittle materials in semiconductor, is an important material removal process that uses free abrasives. Cutting model of single-wire saw machining (SWSM) is the basis of MWSM, and the material removal mechanism of SWSM can better understand than MWSM. Mathematical model (includes brittle fracture and plastic deformation) is presented in this paper for SWSM ceramic with abrasives. This paper determines the effect of various machining parameters on the removal of hard-brittle materials. For brittle fracture of SWSM ceramics, the minimum of the strain energy density is used as a fracture criterion. The material removed of SWSM ceramics due to plastic deformation is calculated using the equations of motion. Actual wire-sawing experiments are conducted to verify the results from the developed mathematical model. Theoretical results agree with experimental data and practical experience. The developed mathematical model shows that brittle fracture plays a major concern role in material removed of SWSM ceramics. Wire speed and working load have positively correlated with material removed of SWSM ceramics. The coefficient of friction is low, a lateral crack, which propagates almost parallel to the working surface, leads to more brittle fracture and material removed is increased on SWSM ceramics.

Keywords: Wire-saw machining; Material removal processing; Brittle fracture; Plastic deformation

*Corresponding authors.

Fax:+886 2 82094845

E-mail: aetcc@mail.lhu.edu.tw (C.C. Tsao); cyhsu@mail.lhu.edu.tw (C.Y. Hsu)

Preprints (www.preprints.org) | NOT PEER-REVIEWED | Posted: 24 August 2020 doi:10.20944/preprints202008.0510.v1

1. Introduction

Ceramics are an important hard-brittle material for the semiconductor and photovoltaic industries. Wire-sawing technology (contains SWSM and MWSM) is the most efficient and economic tool for machining hard-brittle materials, such as silicon, SiC, ceramic and sapphire for the photovoltaic or semiconductor industries [1-3]. A single-wire saw consists of a thin steel wire that is wound around wire-guides, forming a web of parallel wires. The abrasion for single-wire sawing technology can be free or fixed. Wire-saw machining (WSM) is very important work for slicing ceramic ingots. The efficiency of SWSM depends primarily on the cutting action of abrasive particle in the slurry. The ceramic that is removed by the abrasive particles is the major factor in machining efficiency, cost reduction and the quality of the machined surface [4]. Studies [5-6] show that there are both cracks and plastic flow during the cutting of brittle materials. Finnie and McFadden [7] used hard abrasive particles to strike a ductile metal at a low angle and predicted that the volume of material removed is positively correlated to the n^{th} power of speed, for $2<n<3$. Evans [8] showed the impact of each abrasive particle on hard-brittle materials is proportional to the penetration depth of the abrasive particle and the square of the crack length using the elastic-plastic theory. Wang and Rajurkar [9] studied the cutting factors on the material removal rate (MRR) of an ultrasonic machining process. However, the MRR is the amount of weight removed per unit volume of material and is widely used to optimize the wire-sawing process. Slicing ceramics requires a high value for the MRR but the processing conditions must be controlled to avoid instability which causes defects such as cracks, porosity and straying of cutting path.

On the other hand, some studies develop a few material removal models for the wire-sawing process that uses abrasive diamond particles [10-13]. The removal of hard-brittle material during wire-sawing involves plastic deformation and brittle fracture. During SWSM, the stainless steel wire driven abrasives move against rather than strike the work material. Therefore, this present study

Preprints (www.preprints.org) | NOT PEER-REVIEWED | Posted: 24 August 2020 doi:10.20944/preprints202008.0510.v1

determines the theoretical model of MRR for hard-brittle material during SWSM. The governing equations are derived based on the fracture principle of strain energy density (for brittle fracture) and the equation of motion (for plastic deformation), and the effect of various cutting factors (S and P) on material removal is determined. In addition, experiments are conducted for verification the developed theoretical model in this study.

2. Theoretical derivation model

2.1 Mechanism of brittle material removal

The mechanism for the removal hard-brittle material during WSM involves the shear force of the thin film in the slurry and the fine cutting from the rolling and impact of abrasives [14]. The shear force of the thin film and the rolling impact have a limited effect due to large abrasives of about 8~27 μm are used for WSM. When the depth of cut is less than 1 μm, the hard-brittle materials experience ductile-regime grinding [15]. The material experiences plastic deformation due to the plowing of abrasives and piles up either side of the abrasive. Material at the front end of the abrasive cutting edge also undergoes chipping due to plastic deformation. For a depth of cut of 1~4 μm, a lateral crack emerges along with debris [16]. This result is similar to that for scribing indentation [17], in which the pile-up that is generated by plowing function may be removed at the same time.

Figs. 1(a) and 1(b) illustrate the mechanism for the removal hard-brittle materials during SWSM. Fig. 1(a) shows that the material is pushed to the sides and piles up due to plowing by abrasives when the depth of cut is shallow and there is fine chipping at the front end of the abrasives. Fig. 1(b) shows the lateral crack that is formed for a deeper cut, which produces debris and removes a larger quantity of material. The experimental results for driving stainless steel wire to allow SiC slurry to work on a workpiece made of Al_2O_3 are shown in Figs. 2(a) and 2(b). Position A in Fig. 2(a) shows the plastic

Preprints (www.preprints.org) | NOT PEER-REVIEWED | Posted: 24 August 2020 doi:10.20944/preprints202008.0510.v1

deformation and position B shows brittle fracture. In Fig. 2(b) position D denotes the chipping that is generated by brittle fracture. The chip was analyzed using an Energy-dispersive Spectrometer. Fig. 2(c) shows that the chip consists of Al_2O_3, in which Au is tinted for observation by SEM. This study assumes that a minute volume is removed by abrasive slurry, as shown in Fig. 3, wherein zones I and II are the plastic deformation region and the lateral fracture region, respectively. The following descriptions are divided into two parts.

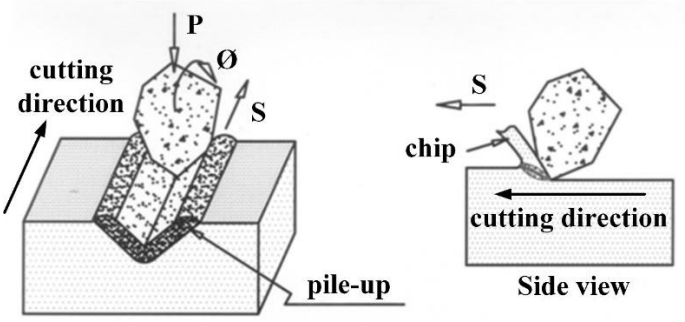

(a)

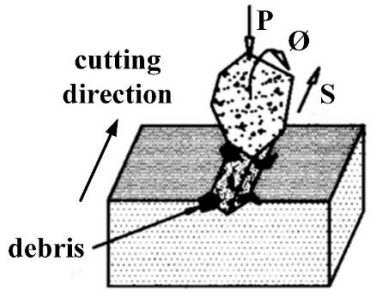

(b)

Fig. 1 Illustration of wire-sawing: (a) fine chips removed by plastic deformation and (b) debris generated by brittle fracture

Preprints (www.preprints.org) | NOT PEER-REVIEWED | Posted: 24 August 2020 doi:10.20944/preprints202008.0510.v1

(a) Plastic deformation at position A and brittle fracture at position B

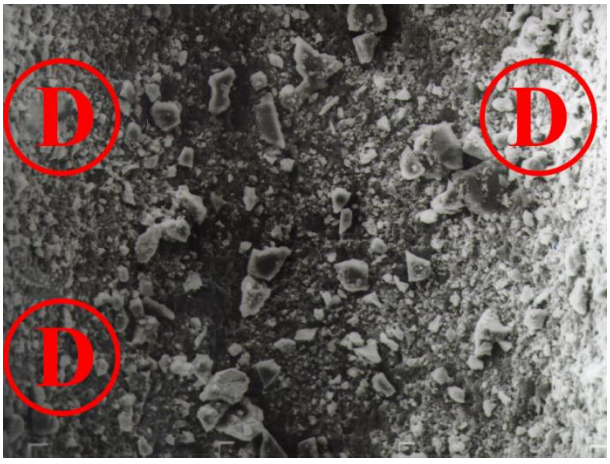

(b) Debris at position D

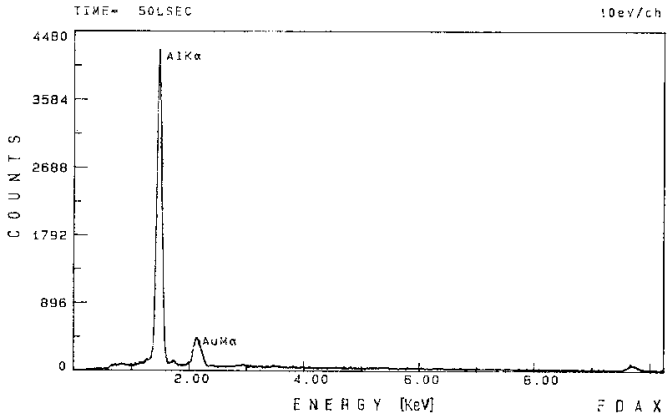

(c) Energy-dispersive Spectrometry results for the debris shown in Fig. 2(b)

Fig. 2 Wire-saw machining of Al_2O_3 using SiC (working load of 1.27 N, wire speed of 2.8 m/s)

Preprints (www.preprints.org) | NOT PEER-REVIEWED | Posted: 24 August 2020 doi:10.20944/preprints202008.0510.v1

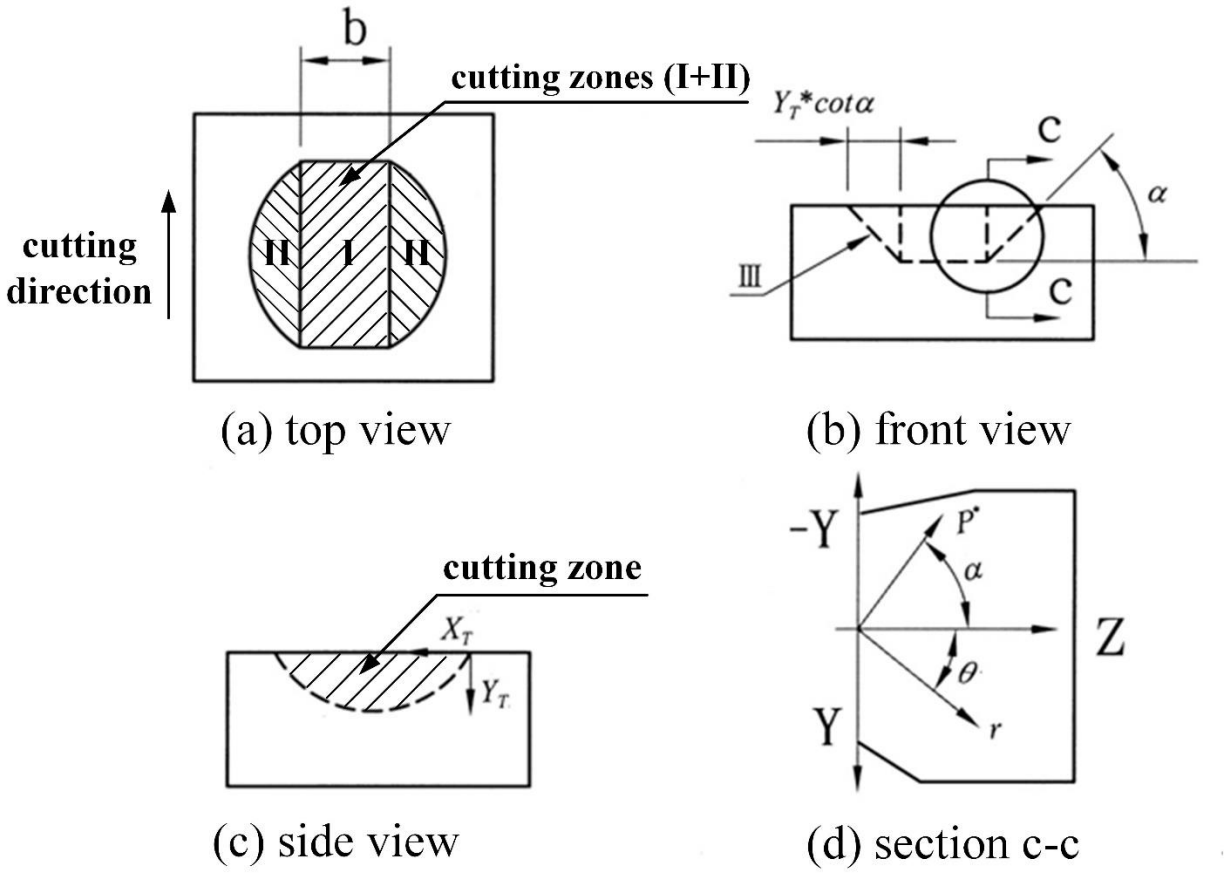

Zone Ⅰ: plastic deformation region

Zone Ⅱ: brittle fracture region

Zone Ⅲ: predicted lateral fracture path

b : cutting width of the abrasive particle

P^* : minimum threshold load for lateral crack

$tan\alpha=\mu$

Fig. 3 Schematic diagram of the volume removed by a single abrasive particle

2.2 Brittle fracture

The stress intensity factor (K), the energy release rate (G) and the J-integral are the parameters that are commonly used to predict fracture within a brittle material. However, they all assume that there is a crack before the analysis. Sih [18] uses the strain energy density criterion to predict fracture initiation and to determine the fracture trajectory. The strain energy density criterion is based on the

Preprints (www.preprints.org) | NOT PEER-REVIEWED | Posted: 24 August 2020 doi:10.20944/preprints202008.0510.v1

global energy field, instead of the local stress or energy field for the failure analysis. This method does not require the assumption that a crack exists. The strain energy density (dW/dV) can be written as follows:

$$\frac{dW}{dV} = \int_0^{\varepsilon_{ij}} \sigma_{ij} d\varepsilon_{ij} \quad (1)$$

where W denotes the total energy that is stored in an element; V denotes the volume of material removed that is removed by an abrasive particle and σ_{ij} and ε_{ij} are the stress and strain vectors, respectively. Using the strain energy density, the location and the instant of fracture initiation require the following basic assumptions [18]:

(1). Fracture initial occurs at the location with the minimum value of (dW/dV), denoted by $(dW/dV)_{\min}$. If there is more than $(dW/dV)_{\min}$, then fracture occurs at the point between the minimum value of $(dW/dV)_{\min}$ and maximum value of $(dW/dV)_{\max}$, denoted by $[dW/dV]_{\min}^{\max}$.

(2). Fracture extension occurs when the (dW/dV) reaches a critical value, denoted by $\left[(dW/dV)\right]_C$.

The local view of the strain energy density of the crack tip uses the polar coordinates, r and θ. The fracture path is predicted based on assumption (1). There is a $[dW/dV]_{\min}^{\max}$ around the specific point for a given r and θ between -90° and 90°. Point A in Fig. 4 is the location where fracture occurs. As r increases gradually, a series of points corresponding to $[dW/dV]_{\min}^{\max}$ are obtained. The fracture path is obtained by connecting these points [19]. There are two different types of crack: a median crack that propagates underneath scribing and a lateral crack, which results in surface fracture. The lateral crack has a significant effect on the removal of brittle material. The minimum threshold load for a lateral crack (P^*) is derived in [16]. In Fig. 3(d), the concentrated forces of the abrasive particle

Preprints (www.preprints.org) | NOT PEER-REVIEWED | Posted: 24 August 2020 doi:10.20944/preprints202008.0510.v1

acting in the Z and $-Y$ directions on the sides of workpiece (Z plane) are $P^*\cos\alpha$ (P_{ZZ}) and $P^*\sin\alpha$ ($-P_{ZY}$), respectively, so the stress in the Z plane, expressed in polar coordinates, is [20]:

$$\sigma_r = \frac{2P^*}{\pi r}\cos(\alpha+\theta) \tag{2}$$

where $tan\alpha = \mu$, and μ denotes the coefficient of friction. The strain energy density is [20]

$$\frac{dW}{dV} = \frac{(1-2\nu^2)}{2E}\sigma_r^2 \tag{3}$$

where ν is Poisson's ratio and E is the modulus of elasticity. Substituting Eq. (2) into Eq. (3) yields:

$$\frac{dW}{dV} = \frac{(1-2\nu^2)}{2E}\left(\frac{2P^*}{\pi r}\right)^2\cos^2(\alpha+\theta) \tag{4}$$

According to the uni-axial tensile test, the critical strain energy density $(dW/dV)_C$ can be represented as:

$$\left(\frac{dW}{dV}\right)_C = \frac{\sigma_U{}^2}{2E} \tag{5}$$

where σ_U is the ultimate material strength. When $[dW/dV]_{min}^{max} = (dW/dV)_C$, the material begins to fracture, so

$$\frac{(1-2\nu^2)}{2E}\left(\frac{2P^*}{\pi r}\right)^2\cos^2(\alpha+\theta_c) = \frac{\sigma_U{}^2}{2E} \tag{6}$$

where θ_c is the angle at which $[dW/dV]_{min}^{max}$ occurs.

Using Eq. (6), for a specific radius r and if θ is –90° to 90°, the location corresponding to $[dW/dV]_{min}^{max}$ can be determined. For coefficients of friction (μ) of 0.1, 0.2, 0.3 and 0.4, the locations for fracture initiation are derived using Eq. (6). The calculated values of θ_c are respectively equal to -5.71°, -11.3°, -16.7° and -21.8°.

Preprints (www.preprints.org) | NOT PEER-REVIEWED | Posted: 24 August 2020 doi:10.20944/preprints202008.0510.v1

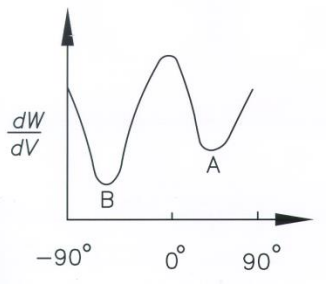

Fig. 4 Illustration of fracture initiation

2.3 Plastic deformation

Fig. 5(a) shows a mass (m) of abrasive particle plowing a trajectory in a ductile material because of its inertial force. Finnie and Mcfadden [7] solved the equations of motion for this particle to predict the volume that is removed by erosion. The equations of motion for abrasive particles are used to derive the volume of plastic deformation, as shown in Eqs. (7)~(9). In Fig. 5(b), the center of mass of the abrasive particle moves parallel to the Z plane and rotates at an angle of ϕ due to the working load (P) that is exerted by the stainless wire and the wire speed (S). The locus left by the abrasive particle tip cutting into the material surface is (X_T, Y_T). The cutting also leads to a plastic deformation chip at the front end.

$$-F_X = mX'' \tag{7}$$

$$-F_Y + P = mY'' \tag{8}$$

$$F_X r = I\phi'' \tag{9}$$

Preprints (www.preprints.org) | NOT PEER-REVIEWED | Posted: 24 August 2020 doi:10.20944/preprints202008.0510.v1

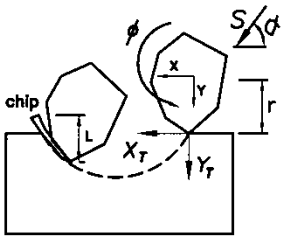

(a) Inertial force only

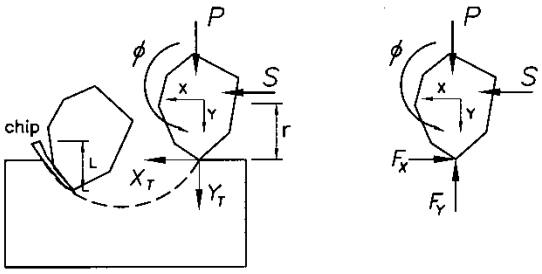

(b) Working load (P) and wire speed (S)

Fig. 5 Schematic diagram of a two-dimensional cutting process using an abrasive particle

The depth of cut is very shallow and the rotational angle is very small, so it is assumed that the movement relative to the abrasive particle tip and the center of mass is $X_T \cong X + r\phi$ and $Y_T = Y$, as shown in Fig. 5(b). The horizontal and vertical cutting forces at the tip of the abrasive particle are F_X and F_Y, respectively, as shown in Fig. 5(b), so the plastic flow stress $\sigma = F_X / A$ is assumed to be constant, where A is the projection area of the contact between the abrasive particle and the chip. However, $A = Lb$, where L is the chip length and b is the width of cut for a single abrasive particle, as shown in Fig. 5(b). From reference [7], $L/Y_T = K = 2$, $F_Y / F_X = J$, where J is a constant.

Using these assumptions, $F_X = \sigma A = \sigma Lb = \sigma bKY_T = \sigma bKY$. Similarly, $F_Y = \sigma bKJY$ and the centroid moment $M_G = \sigma bKrY$. The equations of motion for the abrasive particle are rewritten as:

$$mX'' + \sigma bKY = 0 \qquad (10)$$

Preprints (www.preprints.org) | NOT PEER-REVIEWED | Posted: 24 August 2020 doi:10.20944/preprints202008.0510.v1

$$mY'' + \sigma bKJY = P \tag{11}$$

$$I\phi'' - \sigma bKrY = 0 \tag{12}$$

where m is the mass for a single abrasive particle, as shown in Fig. 3(a), P is the working load, I is the moment of inertia of a particle about its center of gravity and r is the average particle radius, as shown in Fig. 5(b). For the initial conditions, $Y(0) = 0$ and $Y'(0) = 0$, the solution of Eq. (11) is:

$$Y(t) = \left(- \frac{P}{K b \sigma J} \right) \cos \left(\sqrt{\frac{K b \sigma J}{m}} \right) t + \frac{P}{K b \sigma J} \tag{13}$$

By substituting $Y(t)$ into Eq. (10) and using initial conditions $X(0) = 0$ and $X'(0) = S$, then $X(t)$ can be expressed as :

$$X(t) = \left(- \frac{P}{K b \sigma J^2} \right) \cos \left(\sqrt{\frac{K b \sigma J}{m}} \right) t - \frac{P}{2mJ} t^2 + S t + \frac{P}{K b \sigma J^2} \tag{14}$$

By substituting $Y(t)$ into Eq. (12) and using initial values $\phi(0) = 0$ and $\phi'(0) = 0$, the rotation of the particle is:

$$\varphi(t) = \left(\frac{mrP}{K b \sigma I J^2} \right) \cos \left(\sqrt{\frac{K b \sigma J}{m}} \right) t + \frac{rP}{2mJ} t^2 - \frac{mrP}{K b \sigma I J^2} \tag{15}$$

2.4 Material removed by an abrasive particle

The material that is removed by an abrasive particle (V) is calculated by combining the brittle fracture and the plastic deformation as:

$$V = \int b^* Y_T dX_T \tag{16}$$

Preprints (www.preprints.org) | NOT PEER-REVIEWED | Posted: 24 August 2020 doi:10.20944/preprints202008.0510.v1

where $X_T = X(t) + \gamma\phi(t)$

$$Y_T = Y(t)$$

$$b^* = b + 2Y_T(t)\cot\alpha \tag{17}$$

Therefore, the material that is removed is:

$$V = \int [b + 2Y(t)\cot\alpha] Y_T d[X(t) + \gamma\phi(t)] \tag{18}$$

If the tip of the abrasive particle is moving horizontally as it leaves the surface, $Y_T(t) = 0$, so Eq. (10) yields:

$$\cos(Kb\sigma J/m)^{1/2} t = 1$$

or $t = 2\pi/(Kb\sigma J/m)^{1/2}$ (19)

Substituting Eqs. (13), (14), (15) and (19) into Eq. (18), the volume that is removed is written as:

$$V = \left(\frac{mr^2 P}{IK\, b\,\sigma\, J^2} - \frac{P}{Kb\,\sigma\, J^2}\right)\left[\frac{3P}{4K\sigma J} + \frac{5}{3}\left(\frac{P}{Kb\,\sigma\, J}\right)^2 \cot\alpha\right]$$
$$+\left(\frac{P}{mJ} - \frac{r^2 P}{I J}\right)\left[\frac{P}{K\sigma J} + \frac{15}{4}\left(\frac{P}{Kb\sigma J}\right)^2 \cot\alpha\right]\frac{m}{Kb\,\sigma\, J}$$
$$+\left[\left(\frac{r^2 P}{I J} - \frac{P}{m J}\right)\left(\frac{P}{Kb\sigma J}\right)^2 \cot\alpha + \left(\frac{P}{K\sigma J} + 3\left(\frac{P}{Kb\sigma J}\right)^2 \cot\alpha\right)\right]\frac{2\pi S}{\sqrt{Kb\,\sigma\, J/m}}$$
$$+\left(\frac{r^2 P}{I J} - \frac{P}{mJ}\right)\left[\frac{P}{2K\sigma J} + \frac{1}{2}\left(\frac{P}{K\, b\sigma\, J}\right)^2 \cot\alpha\right]\left(\frac{2\pi}{\sqrt{Kb\,\sigma\, J/m}}\right)^2$$

$I \cong mr^2$, so the material that is removed is written more simply as follows:

Preprints (www.preprints.org) | NOT PEER-REVIEWED | Posted: 24 August 2020 doi:10.20944/preprints202008.0510.v1

$$V = \left[\frac{P}{K\sigma J} + 3\left(\frac{P}{Kb\,\sigma J} \right)^2 \cot\alpha \right] \frac{2\pi S}{\sqrt{Kb\,\sigma Jm}}$$

$\sigma = F_X / A$, $L/Y_T = K = 2$, $\tan\alpha = \mu$ and $F_Y / F_X = J$, so:

$$V = \left[\left(\frac{A\,P}{2F_Y} \right) + \frac{3}{\mu} \left(\frac{A\,P}{2bF_Y} \right)^2 \right] \frac{2\pi S}{\sqrt{2bF_Y/mA}} \tag{20}$$

This equation consists of two parts: for a plastic deformation and for a brittle fracture. The material removal increases as the wire speed (S) and working load (P).

3. Experimental results and discussion

Experiments were conducted to test the proposed theory. The workpiece swings back and forth, as shown in Fig. 6. This vibrating machining model evenly distributes the cutting force of each active grain and makes the disposal of chips more efficient. The main experimental parameters and their values are listed in Table 1. To derive a more precise correlation between the machining parameters and the material that is removed, Eq. (20) is expressed in non-dimensional form as:

$$\left(\frac{V\sqrt{2bF_Y\ /mA}}{2\pi S} \right) \Big/ \left(\frac{AP}{2F_Y} \right) = 1 + \frac{3}{\mu} \left(\frac{AP}{2F_Y} \right) \frac{1}{b^2} \tag{21}$$

Let $N_X = 1 + \frac{3}{\mu} \left(\frac{AP}{2F_Y} \right) \frac{1}{b^2}$ and $N_Y = \left(\frac{V\sqrt{2bF_Y\ /mA}}{2\pi S} \right) \Big/ \left(\frac{AP}{2F_Y} \right)$.

For a single abrasive particle (GC# 600), the width of cut b ($D/3$) is about 9 μm, where D is the diameter, which is 27 μm, and the mass m ($\pi\rho D^3/6$) is 2×10^{-11} kg, where ρ is the density,

Preprints (www.preprints.org) | NOT PEER-REVIEWED | Posted: 24 August 2020 doi:10.20944/preprints202008.0510.v1

with a value of 3.22 g/cm^3. If μ=0.3 [21], $F_Y / F_X = J \cong 1$ [7], the plastic flow stress σ for Al_2O_3 is about 400 MPa, chip length is L ($1.1b$) and the horizontal cutting force F_X is ($\sigma bL = 0.0356N$). For a single abrasive particle, the working load is P (total working load/n_0), so if a_0 is the total area of the machining zone (See Fig. 6), the maximum number of particles that participate in the operation is calculated by dividing the area of the grit by the largest cross-section a_0 ($L_0 b_0$), where L_0 is the line contact length and b_0 is the line width. Accounting for tiny gaps between the grit, the total number of particles n_0 is: $n_0 = C_0 a_0 / (\pi D^2 / 4)$, where C_0 is the gap coefficient, which has a value of 10~20%.

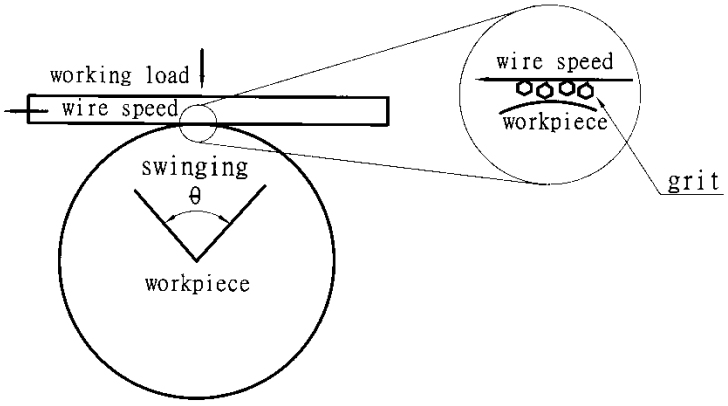

Fig. 6 Model of a swinging wire-sawing

Preprints (www.preprints.org) | NOT PEER-REVIEWED | Posted: 24 August 2020 doi:10.20944/preprints202008.0510.v1

Table 1 Experimental conditions

Item	Specification
Workpiece (Diameter)	Al_2O_3 (ϕ8 mm)
Slurry contents	SiC + Water
Grains (Diameter)	GC# 600 (27μm)
Concentration (wt. %)	10
Wire diameter (mm)	$\phi 0.24 \pm 0.05$ (Stainless wire)
Wire tension (N)	18
Wire speed (m/s)	1.9, 2.8, 4.1, 5.6 and 6.4
Working load (N)	0.90, 1.27 and 1.76
Frequency (Hz)	0.8
Vibration angle (θ)	60º

The material V that is removed by a single abrasive particle is V_0 / n_1, where $V_0 = A_0 w$ denotes the total volume that is removed per unit of time, where A_0 is the cutting area per unit time and w is the kerf width. n_1. ($C_1 S n_0 / L_0$) denotes the total number of machining abrasives per unit time, where C_1 is the wire speed coefficient, which has a value of 70~90%, and S is the wire speed. The experimental conditions and results are listed in Table 2, which is used to produce the chart in Fig. 7. The figure shows that the experimental values with different wire speeds (4.1 m/s (●), 5.6 m/s (■) or 6.4 m/s (▲)), all have an approximate linear relationship, which is very close to the format for theoretical Eq. (18). However, if the working load is increased, the clearance between the wire and the surface of the workpiece decreases, which prevents the abrasive grains from entering the working area, so the experimental material removal rate is lower than the theoretical value.

Table 2 Experimental conditions and results

	P (N)	S (m/s)	V	N_X	N_Y

Preprints (www.preprints.org) | NOT PEER-REVIEWED | Posted: 24 August 2020 doi:10.20944/preprints202008.0510.v1

a	0.6	4.1	1.31E-7	2.325	3.550
	0.6	5.6	1.41E-7	2.325	2.791
	0.6	6.4	1.10E-7	2.325	2.428
b	0.9	4.1	2.04E-7	2.990	3.680
	0.9	5.6	2.08E-7	2.990	2.750
	0.9	6.4	2.14E-7	2.990	2.480
c	1.12	4.1	2.69E-7	3.474	3.900
	1.12	5.6	2.76E-7	3.474	2.940
	1.12	6.4	2.72E-7	3.474	2.610
d	1.27	4.1	3.20E-7	3.805	4.100
	1.27	5.6	3.40E-7	3.805	3.197
	1.27	6.4	3.47E-7	3.805	2.850
e	1.76	4.1	5.00E-7	4.887	4.570
	1.76	5.6	5.10E-7	4.887	3.880
	1.76	6.4	5.10E-7	4.887	3.040
f	1.96	4.1	5.70E-7	5.330	4.710
	1.96	5.6	6.30E-7	5.330	4.010
	1.96	6.4	6.25E-7	5.330	3.270

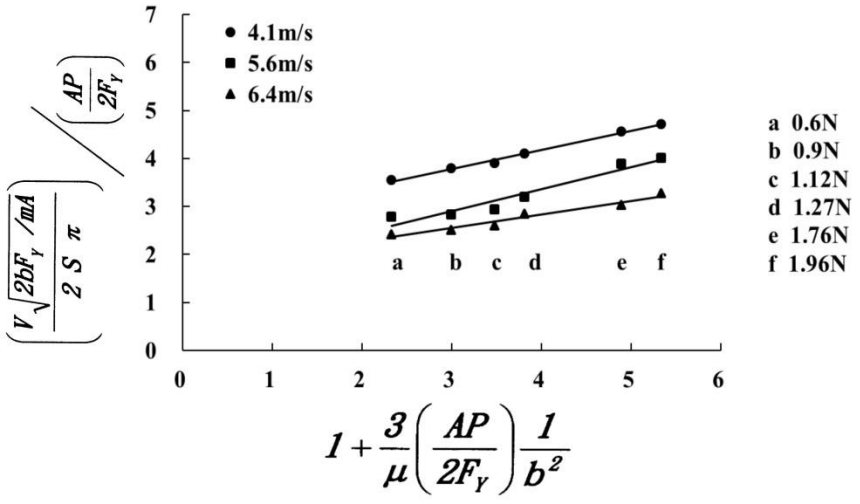

Fig. 7 Experimental results for the volume of Al_2O_3 that is removed

Preprints (www.preprints.org) | NOT PEER-REVIEWED | Posted: 24 August 2020 doi:10.20944/preprints202008.0510.v1

The N_Y value for 5.6 m/s (■) is lower than 4.1 m/s (●) because the volume that is removed by one single abrasive is $V = V_0 / n_1$, where V_0 denotes the total volume removed per unit time, n_1 denotes the total number of machining abrasives per unit time and $n_1 = C_1 S n_0 / L_0$. The speed of the wire-saw is unknown, so the ratio of the speed to the total number of machining abrasives per unit of time (n_1) is assumed to be 1:1. Therefore, the faster the wire, the greater is the value of n_1 and the smaller is the volume that is removed by a single abrasive (V). The 5.6 m/s (■) value at a high wire speed is lower than the 4.1 m/s (●) value at a low wire speed. The result verifies the equation for the material that is removed by a single abrasive Eq. (20).

Eq. (20) allows the contribution of the material that is removed by plastic deformation to be determined. This is plotted as a dashed line in Fig. 8. A small amount of material is removed by plastic deformation and brittle fracture plays the dominant role. This is reasonable since there is only ductile flow when the depth of cut is less than 1 μm [16]. For this study, the depth of cut (from Eq. (10)) is 0.5 μm to 4 μm, so there is lateral cracking and plastic flow. Fig. 9 shows the relationship between the working load and the ratio of brittle/ductile removal rates. Increasing the working load increases the depth of cut so there is more evidence of lateral brittle fracture and the kerf width increases. For wire-saw machining, the MRR is increased when the working load (P) is increased. If the working load exceeds a threshold, the steel wire can break easily. The cutting path can also become crooked. Therefore, the working load must not exceed a specified threshold value. If the wire speed (S) is increased, the amount of grains that enters the machining zone from the slurry within a specific time increases, so significantly more material is removed.

From Eq. (20), the larger the grit size A, the greater is the machining efficiency. However, it the surface roughness of the wafer also increases. Suwabe et al. [22] showed that the addition of smaller grains in the slurry results in a smoother wafer. However, when all of the particles in the

Preprints (www.preprints.org) | NOT PEER-REVIEWED | Posted: 24 August 2020 doi:10.20944/preprints202008.0510.v1

slurry are smaller than #1000, a further increase in the working load or the wire speed produces no increase is the volume that is removed. Fig. 10 shows the theoretical values for material removed for abrasives of mesh size #600 (solid line) and size #1000 (dash line). there is no difference in the amount of material that is removed when the grit is too small. The higher the material hardness, the greater is the normal cutting force (F_Y), so the MRR is decreased. Higher material hardness results in brittle fracture of the material. The coefficient of friction has an effect on crack propagation [23]. Fig. 3(b) shows that when the coefficient of friction coefficient decreases, a lateral crack propagates almost parallel to the specimen surface. This results in brittle fracture and more material is removed. This is confirmed by Eq. (20).

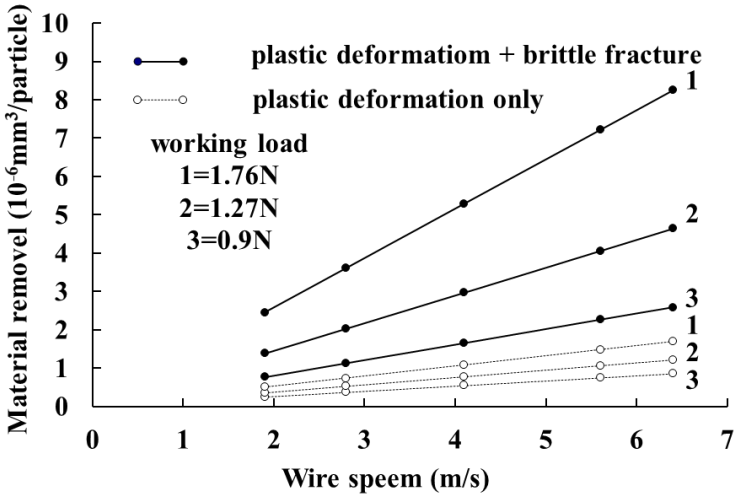

Fig. 8 Theoretical value for material that is removed by a single grit

Preprints (www.preprints.org) | NOT PEER-REVIEWED | Posted: 24 August 2020 doi:10.20944/preprints202008.0510.v1

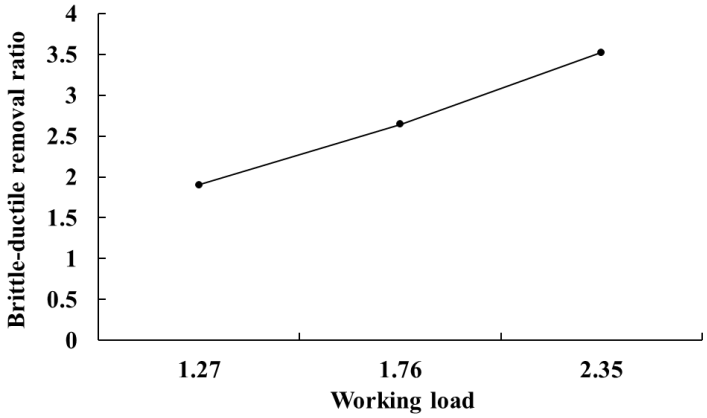

Fig. 9 Ratio of brittle fracture to ductile removal rate

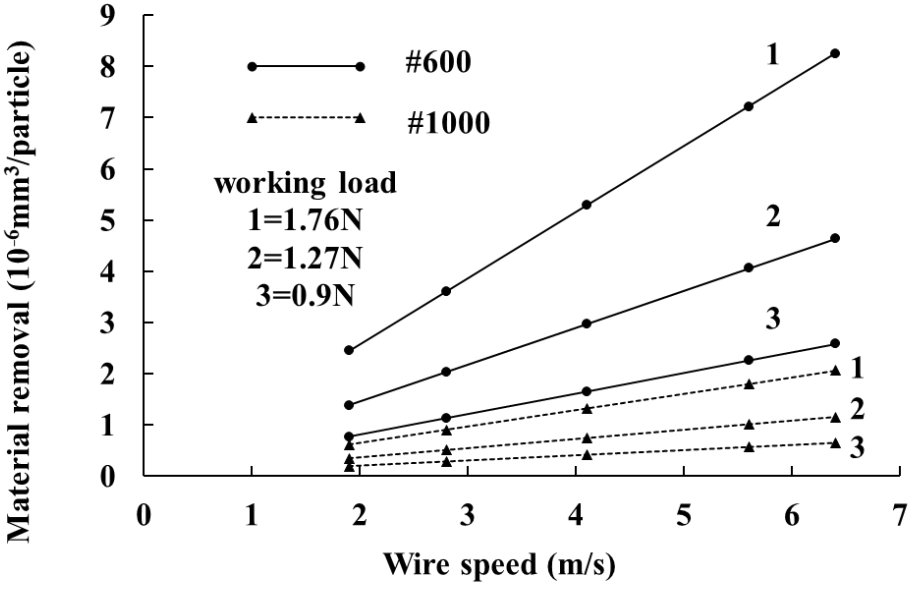

Fig. 10 Material removed by different size of grit

4. Conclusion

Slicing ceramic technology using WSM still has disadvantages in terms of the MRR deviation. However, WSM increases productivity and the MRR for slicing ceramics, which decreases the

Preprints (www.preprints.org) | NOT PEER-REVIEWED | Posted: 24 August 2020 doi:10.20944/preprints202008.0510.v1

manufacturing cost. A mathematical model for material removal for SWSM of brittle material is derived and the effect of important parameters on the material removal is determined. The material removal of SWSM involves plastic deformation and brittle fracture. Actual SWSM experiments on MRR are conducted to verify the results from the mathematical model study. The theoretical results agree with experimental data and practical experience. An increase in the wire speed (S) and working load (P) results in the removal of more material, but increasing the working load also increases the kerf width.

Nomenclature:

a_0	Total area of the machining zone
b	Cutting width for a single abrasive particle
b_0	Line width
m	Mass of the abrasive particle
n_0	Total number of particles
n_1	Total number of machining abrasives per unit time
r	Average particle radius
w	Kerf width
A	Projection area of the contact between the abrasive particle and the chip
A_0	Cutting area per unit time
C_0	Gap coefficient
C_1	Wire speed coefficient
D	Diameter of a single abrasive particle
E	Modulus of elasticity
F_X	Horizontal cutting force for the tip of an abrasive particle
F_Y	Vertical cutting force for the tip of an abrasive particle
I	Moment of inertia of a particle about its center of gravity

L	Chip length
L_0	Line contact length
M_G	Centroid moment
P	Working load
P^*	Minimum threshold load for lateral cracking
S	Wire speed
V	Volume of material that is removed by an abrasive particle
V_0	Total volume that is removed per unit time
W	Total energy stored in an element
X_T, Y_T	Locus left by the tip of an abrasive particle cutting into the material surface
ε_{ij}	Strain vector
σ	Plastic flow stress
σ_{ij}	Stress vector
σ_r	Stress in the Z plane
σ_U	Ultimate material strength
μ	Coefficient of friction
ν	Poisson's ratio
θ_c	Angle at which $[dW/dV]_{\min}^{\max}$ occurs
ρ	Density of a single abrasive particle

Acknowledgement

The authors would like to express their appreciation to Kinik Company for providing the slurry used in this study. The authors gratefully acknowledge the support of the Ministry of Science and Technology of the Republic of China, through Grant nos. MOST 108-2622-E-262-006-CC3.

References

[1] T. Liedke, M. Kuna, Discrete element simulation of micromechanical removal processes during wire sawing, Wear 304 (2013) 77-82.

[2] X. Y. Li, Y. F. Gao, P. Q. Ge, L. Zhang, W. B. Bi, The effect of cut depth and distribution for abrasives on wafer surface morphology in diamond wire sawing of PV polycrystalline silicon, Mater. Sci. Semicond. Process 91 (2019) 316-326

[3] H. P. Xiao, H. R. Wang, N. Yu, R. G. Liang, Z. Tong, Z. Chen, J. H. Wang, Evaluation of fixed abrasive diamond wire sawing induced subsurface damage of solar silicon wafers, J. Mater. Process. Technol. 273 (2019) 116267.

[4] A. Bidiville, K. Wasmer, M. Van der Meer, C. Ballif, Wire-sawing processes: parametrical study and modeling, Sol. Energy Mater. Sol. Cells 132 (2015) 392-402.

[5] B. Zhang, T. D. Howes, Material-removal mechanisms in grinding ceramics, Ann. CIRP 43 (1) (1994) 305-308.

[6] T. C. Buttery, J. F. Archard, Grinding and abrasive wear, Proc. Inst. Mech. Eng. 185 (1970) 537-551.

[7] I. Finnie, D. H. Mcfadden, On the velocity dependence of the erosion of ductile metals by solid particles at low angles of incidence, Wear 48 (1978) 181-190.

[8] A. G. Evans, Impact damage in ceramic, Frac. Mech. Ceram., 3 (1978) 303-330.

[9] Z. Y. Wang, K. P. Rajurkar, Dynamic analysis of the ultrasonic machining process, ASME J. Manu. Sci. Eng., 118 (1996) 376-381.

[10] T. Liedke, M. Kuna, A macroscopic mechanical model of the wire sawing process, Int. J. Mach. Tools Manuf. 51 (2011) 711-720.

[11] T. Y. Liu, P. Q. Ge, W. B. Bi, Y. F. Gao, Subsurface crack damage in silicon wafers induced by resin bonded diamond wire sawing, Mater. Sci. Semicond. Process 57 (2017) 147-156.

[12] P. Z. Wang, P. Q. Ge, Y. F. Gao, W. B. Bi, Prediction of sawing force for single-crystal silicon

carbide with fixed abrasive diamond wire saw, Mater. Sci. Semicond. Process 63 (2017) 25-32.

[13] P. Z. Wang, P. Q. Ge, M. R. Ge, W. B. Bi, J. F. Meng, Material removal mechanism and crack propagation in single scratch and double scratch tests of single-crystal silicon carbide by abrasives on wire saw, Ceram. Int. 45 (2019) 384-393.

[14] Y. T. Su, S. Y. Wang, J. S. Hsiau, On machining rate of hydrodynamic polishing process, Wear 188(1995), 77-87.

[15] T.G. Bifano, T. A. Dow, R. O. Scattergood, Ductile-regime grinding: a new technology for machining brittle materials, ASME, J. Eng. Ind., 113, (1991) 185-188.

[16] S. Malkin, T. W. Hwang, Grinding mechanisms for ceramics, Ann. CIRP 45 (2) (1996) 569-580.

[17] S. Y. Chen, T. N. Farris, S. Chandrasekar, Sliding microindentation fracture of brittle materials, Tribol. Trans., 34 (2) (1991) 161-168.

[18] G. C. Sih, Mechanics of fracture initiation and propagation, Kluwer Academic Publishers, The Netherlands (1991).

[19] C. K. Chao, R. C. Chang, Crack trajectories influenced by mechanical and thermal disturbance in anisotropic material, J. Theoret. Appl. Fracture Mech. 17 (1992) 177-187.

[20] S. P. Timoshenko, J. N. Goodier, Theory of elasticity, McGraw-Hill (1970).

[21] A. Krell, D. Klaffke, Effect of grain size and Humidity on fretting wear in fine-grained alumina, Al_2O_3/Tic, and Zirconia, J. Am. Ceram. Soc. 79 (5) (1996)1139-1146.

[22] H. Suwabe, K. I. Ishikawa, T. Miyashita, A study of the processing characteristics of a vibration multi-wire saw-regarding the effects of slurry composition, Int. Conf. Precis. Eng., Taipei (1997) 253-256.

[23] A. F. Bower, N. A. Fleck, Brittle fracture under a sliding line contact, J. Mech. Phys. Solids 42 (1994) 1375-1396.